Computation of Lightning Electromagnetic Pulses Using the Constrained Interpolation Profile Method

K. Kajita, Y. Baba, N. Nagaoka, A. Akihiro

***Abstract*-- In this paper, a numerical procedure for computing electric and magnetic fields in a three-dimensional space using the constrained interpolation profile (CIP) method is presented. Then, this method is applied to computing electric and magnetic fields, which are generated by a current wave propagating upward along a vertical lightning return-stroke channel. The lightning return-stroke channel is modeled by a phased-current-source array. The spatial and temporal distribution of the lightning return-stroke channel or phase-current-source array is represented by a new simple mathematical function of height, time and channel-based current.**

***Keywords*: Constrained interpolation profile method, electromagnetic field, finite-difference time-domain method, lightning channel model.**

I. Introduction

RECENTLY, electromagnetic computation methods have been used frequently in analyzing lightning electromagnetic pulses and surges [1]. Among electromagnetic computation methods, the finite-difference time-domain (FDTD) method [2] and the method of moments (MoM) [3] have been most frequently used. Therefore, their fundamental theories, advantages and disadvantages are familiar to researchers related. On the other hand, methods other than these two are little known.

In this paper, a numerical procedure for computing electromagnetic fields in a three-dimensional (3D) space using the constrained interpolation profile (CIP) method [4] is presented. Although the CIP method has been employed in numerical computations in Hydromechanics, it is a sort of new methods in lightning electromagnetic-pulse and surge computations. Then, this method is applied to computing electromagnetic fields, which are generated by a current wave propagating upward along a vertical lightning return-stroke channel located on flat perfectly conducting ground, and the CIP-computed waveforms are compared with the corresponding waveforms computed using the FDTD method. The lightning return-stroke channel is modeled by a phased-current-source array. The spatial and temporal distribution of the lightning channel is represented by a new simple mathematical function of height, time and channel-based current.

The authors are with the Department of Electrical Engineering Doshisha University, Kyoto 610-0321, Japan(E-mail;ybaba@mail.doshisha.ac.jp).

Paper submitted to the International Conference on Power Systems Transients (IPST2013) in Vancouver, Canada July 18-20, 2013.

II. The Theory Of The CIP Method

A. Fundamentals

The CIP method is one of the finite-difference methods, which was proposed by Yabe et al. [4]. The advection equation for one-dimensional spatial-variable function $f(x, t)$ is given by

$$\frac{\partial f}{\partial t} + u\frac{\partial f}{\partial x} \quad \cdots\cdots(1)$$

where u is the propagation velocity of a wave of interest.

As one of the schemes for numerically solving Eq. (1), the upwind finite-difference scheme is known. However, the use of this scheme causes numerical dispersion as shown in Fig. 1, when a relatively coarse grid is used. Differently from the upwind finite-difference method, the CIP method considers not only electric- and magnetic-field values on grid points but also their derivative values there. In principle, therefore, it can suppress numerical dispersions even when a relatively coarse grid is used.

The CIP method employs an additional advection equation for spatial derivative given below.

$$\frac{\partial g}{\partial t} + u\frac{\partial g}{\partial x} = 0 \quad \cdots\cdots(2)$$

where $g = \partial f / \partial x$.

The use of Eqs. (1) and (2) allows one to simulate the propagation of a wave with a less numerical dispersion as shown in Fig. 2. This method has been successfully used in numerical computations in Hydromechanics.

In the CIP method, the profile of function f of x between grid points i-1 and i is approximated by a cubic function given below.

$$F_i(x,t) = a_i(x-x_i)^3 + b_i(x-x_i)^2 + c_i(x-x_i) + d_i \quad \cdots\cdots(3)$$

Coefficients, a_i, b_i, c_i, and d_i, are determined from values of f, which are f_{i-1} and f_i, at grid points i-1 and i, respectively, and values of spatial derivative of f, which are $g_{i-1}=\partial f_{i-1}/\partial x$ and $g_i=\partial f_i/\partial x$, at the same grid points. They are given as follows.

$$a_i = \frac{g_i + g_{i-1}}{(-\Delta x)^2} + \frac{2(f_i - f_{i-1})}{(-\Delta x)^3} \quad \cdots\cdots (4)$$

$$b_i = \frac{3(f_{i-1} - f_i)}{(-\Delta x)^2} - \frac{2g_i + g_{i-1}}{(-\Delta x)} \quad \cdots\cdots (5)$$

$$c_i = g_i \quad \cdots\cdots (6)$$

$$d_i = f_i \quad \cdots\cdots (7)$$

By computing time-update equations (8) and (9), coefficients of which are given by Eqs. (4) to (7), f_i^{n+1} and g_i^{n+1} at the next step $n + 1$ are obtained.

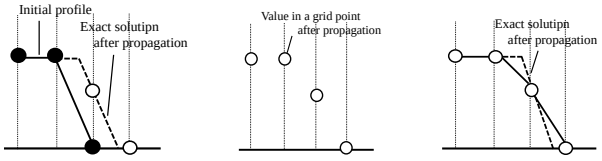

(a) Initial profile (b) Value in grid points (c) Distorted profile

Fig. 1. Conceptual picture of the upwind finite-difference scheme and its resultant numerical dispersion.

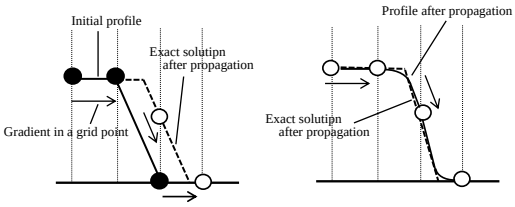

(a) Initial profile (b) Exact solution after propagation

Fig. 2. Conceptual picture of the CIP interpolation.

$$f_i^{n+1} = a_i\xi^3 + b_i\xi^2 + g_i^n\xi + f_i^n \quad \cdots\cdots(8)$$

$$g_i^{n+1} = 3a_i\xi^2 + 2b_i\xi + g_i^n \quad \cdots\cdots(9)$$

where ξ is $-u\Delta t$.

Note that the above-explained procedure is for a wave propagating at a constant speed of u in the positive direction of x. For simulating a wave propagating in the negative direction, Eqs. (10) and (11) need to be employed instead of Eqs. (4) and (5).

$$a_i = \frac{g_i + g_{i+1}}{\Delta x^2} + \frac{2(f_i - f_{i+1})}{\Delta x^3} \quad \cdots\cdots(10)$$

$$b_i = \frac{3(f_{i+1} - f_i)}{\Delta x^2} - \frac{2g_i + g_{i+1}}{\Delta x} \quad \cdots\cdots(11)$$

B. Application to EM-field computation [5][6]

Faraday's and Ampere's laws are given by

$$\nabla \times \boldsymbol{E} = -\mu\frac{\partial \boldsymbol{H}}{\partial t} \quad \cdots\cdots(12)$$

$$\nabla \times \boldsymbol{H} = \varepsilon\frac{\partial \boldsymbol{E}}{\partial t} + \boldsymbol{J} \quad \cdots\cdots(13)$$

where $\boldsymbol{E}$ is the electric field, $\boldsymbol{H}$ is the magnetic field, $\boldsymbol{J}$ is the conduction-current density, μ is permeability, and ε is permittivity.

When the medium of interest is non-conducting ($\boldsymbol{J} = 0$), Eqs. (12) and (13) are expressed as

$$\frac{\partial \boldsymbol{W}}{\partial t} + \boldsymbol{A}\frac{\partial \boldsymbol{W}}{\partial x} + \boldsymbol{B}\frac{\partial \boldsymbol{W}}{\partial y} + \boldsymbol{C}\frac{\partial \boldsymbol{W}}{\partial z} = 0 \quad \cdots\cdots(14)$$

where $\boldsymbol{W} = (E_x, E_y, E_z, \zeta H_x, \zeta H_y, \zeta H_z)^T$, $\zeta = (\mu/\varepsilon)^{1/2}$. When the propagation velocity of an electromagnetic wave is equal to $c = (\varepsilon\mu)^{-1/2}$, coefficients, $\boldsymbol{A}$, $\boldsymbol{B}$, and $\boldsymbol{C}$ are given by

$$A = \begin{pmatrix} 0 & 0 & 0 & 0 & 0 & 0 \\ 0 & 0 & 0 & 0 & 0 & c \\ 0 & 0 & 0 & 0 & -c & 0 \\ 0 & 0 & 0 & 0 & 0 & 0 \\ 0 & 0 & -c & 0 & 0 & 0 \\ 0 & c & 0 & 0 & 0 & 0 \end{pmatrix} \quad B = \begin{pmatrix} 0 & 0 & 0 & 0 & 0 & -c \\ 0 & 0 & 0 & 0 & 0 & 0 \\ 0 & 0 & 0 & c & 0 & 0 \\ 0 & 0 & c & 0 & 0 & 0 \\ 0 & 0 & 0 & 0 & 0 & 0 \\ -c & 0 & 0 & 0 & 0 & 0 \end{pmatrix} \quad C = \begin{pmatrix} 0 & 0 & 0 & 0 & c & 0 \\ 0 & 0 & 0 & -c & 0 & 0 \\ 0 & 0 & 0 & 0 & 0 & 0 \\ 0 & -c & 0 & 0 & 0 & 0 \\ c & 0 & 0 & 0 & 0 & 0 \\ 0 & 0 & 0 & 0 & 0 & 0 \end{pmatrix}$$

Although Eq. (14) seems to be somewhat unfamiliar, its first element is

$$\frac{\partial E_x}{\partial t} + (-c)\left(\frac{\mu}{\varepsilon}\right)^{\frac{1}{2}}\frac{\partial H_z}{\partial y} + c\left(\frac{\mu}{\varepsilon}\right)^{\frac{1}{2}}\frac{\partial H_y}{\partial z} = 0$$

Therefore, it reduces to

$$\frac{\partial H_z}{\partial y} - \frac{\partial H_y}{\partial z} = \varepsilon\frac{\partial E_x}{\partial t}$$

This apparently shows x-component of Eq. (12), Faraday's law.

Eq. (14) is separated into x-, y-, and z-directions, as given in Eqs. (15), (16), and (17), so that Eqs. (8) and (9) could be applied to.

$$\frac{\partial \boldsymbol{W}}{\partial t} + \boldsymbol{A}\frac{\partial \boldsymbol{W}}{\partial x} = 0 \quad \left(\boldsymbol{W}^n \rightarrow \boldsymbol{W}^*\right) \quad \cdots\cdots(15)$$

$$\frac{\partial \boldsymbol{W}}{\partial t} + \boldsymbol{B}\frac{\partial \boldsymbol{W}}{\partial y} = 0 \quad \left(\boldsymbol{W}^* \rightarrow \boldsymbol{W}^{**}\right) \quad \cdots\cdots(16)$$

$$\frac{\partial \boldsymbol{W}}{\partial t} + \boldsymbol{C}\frac{\partial \boldsymbol{W}}{\partial z} = 0 \quad \left(\boldsymbol{W}^{**} \rightarrow \boldsymbol{W}^{***}\right) \quad \cdots\cdots(17)$$

where $\boldsymbol{W}^n$ indicates $\boldsymbol{W}$ at time step n, $\boldsymbol{W}^*$ indicates $\boldsymbol{W}$ after the calculation of Eq. (15), $\boldsymbol{W}^{**}$ indicates $\boldsymbol{W}$ after the calculation of Eq. (16), and $\boldsymbol{W}^{***}$ indicates $\boldsymbol{W}$ after the calculation of Eq. (17).

When a current source $\boldsymbol{J}$ is present, Eq. (18) needs to be added to the above procedure.

$$\boldsymbol{E}^{n+1} = \boldsymbol{E}^{***} - \Delta t\frac{\boldsymbol{J}^n}{\varepsilon} \quad \left(\boldsymbol{W}^{***} \rightarrow \boldsymbol{W}^{n+1}\right) \quad \cdots\cdots(18)$$

From procedures given from (15) to (18), $\boldsymbol{W}^{n+1}$ in time step n+1 is computed from its previous values $\boldsymbol{W}^n$.

From Eq. (15), electric- and magnetic-field components, which propagate in the direction of x, are expressed as follows.

$$\frac{\partial E_y}{\partial t} - c\zeta\frac{\partial H_z}{\partial x} = 0 \quad \cdots\cdots(19)$$

$$\zeta\frac{\partial H_z}{\partial t} - c\frac{\partial E_y}{\partial x} = 0 \quad \cdots\cdots(20)$$

$$\frac{\partial E_z}{\partial t} - c\zeta\frac{\partial H_y}{\partial x} = 0 \quad \cdots\cdots(21)$$

$$\zeta\frac{\partial H_y}{\partial t} - c\frac{\partial E_z}{\partial x} = 0 \quad \cdots\cdots(22)$$

When Eq. (19) is added to and subtracted from Eq. (20), and Eq. (21) is added to and subtracted from Eq. (22), the following equations are obtained.

$$\frac{\partial(E_y \pm \zeta H_z)}{\partial t} \pm c\frac{\partial(E_y \pm \zeta H_z)}{\partial x} = 0 \quad \cdots\cdots(23)$$

$$\frac{\partial(E_z \pm \zeta H_y)}{\partial t} \mp c\frac{\partial(E_z \pm \zeta H_y)}{\partial x} = 0 \quad \cdots\cdots(24)$$

Similarly, the corresponding equations for their spatial derivatives are obtained as follows.

$$\frac{\partial(\partial_x E_y \pm \zeta\partial_x H_z)}{\partial t} \pm c\frac{\partial(\partial_x E_y \pm \zeta\partial_x H_z)}{\partial x} = 0 \quad \cdots\cdots(25)$$

$$\frac{\partial(\partial_x E_z \pm \zeta\partial_x H_y)}{\partial t} \mp c\frac{\partial(\partial_x E_z \pm \zeta\partial_x H_y)}{\partial x} = 0 \quad \cdots\cdots(26)$$

where $\partial_x = \partial/\partial_x$.

Eqs. (23), (24), (25), and (26) are pure advection equation for $(E_y \pm \zeta H_z)$, $(E_z \pm \zeta H_y)$, $(\partial_x E_y \pm \zeta\partial_x H_z)$ and $(\partial_x E_z \pm \zeta\partial_x H_y)$, respectively. Therefore, their propagations in the direction of x can be solved by applying the CIP method to these equations.

In the same manner as the above, from Eq. (16), pure

advection equations in the direction of y for ($E_x \pm \zeta H_z$), ($E_z \pm \zeta H_x$), ($\partial_y E_y \pm \zeta \partial_y H_z$) and ($\partial_y E_z \pm \zeta \partial_y H_x$) are obtained, and from Eq. (17), pure advection equations in the direction of z for ($E_x \pm \zeta H_y$), ($E_y \pm \zeta H_x$), ($\partial_z E_x \pm \zeta \partial_z H_y$) and ($\partial_z E_y \pm \zeta \partial_z H_x$) are obtained.

Note that, since the above-explained procedures yield spatial derivatives in their propagation direction only, spatial derivatives in directions perpendicular to their propagation direction are computed using the upwind finite-difference scheme.

The flowchart for calculating electric and magnetic fields and their spatial derivatives using the CIP method is shown in Table I.

TABLE I
FLOWCHART FOR COMPUTING ELECTRIC AND MAGNETIC FIELDS AND THEIR SPATIAL DERIVATIVES USING THE CIP METHOD [5]

Step	Physical quantities to be calculated	Equation used
1	E_y, E_z, H_y, H_z, $\partial_x E_y$, $\partial_x E_z$, $\partial_x H_y$,	Eq. (15) : CIP method
1'	$\partial_x H_z$ $\partial_y E_z$, $\partial_z E_y$, $\partial_y H_z$, $\partial_z H_y$	1st-order upwind scheme
2	E_x, E_z, H_x, H_z, $\partial_y E_x$, $\partial_y E_z$, $\partial_y H_x$,	Eq. (16) : CIP method
2'	$\partial_y H_z$ $\partial_z E_x$, $\partial_x E_z$, $\partial_z H_x$, $\partial_z H_x$	1st-order upwind scheme
3	E_x, E_y, H_x, H_y, $\partial_z E_x$, $\partial_z E_y$, $\partial_z H_x$,	Eq. (17) : CIP method
3'	$\partial_z H_y$ $\partial_y E_x$, $\partial_x E_y$, $\partial_y H_x$, $\partial_x H_y$	1st-order upwind scheme

III. LEMP COMPUTATIONS USING DIFFERENT ENGINEERING LIGHTNING RETURN-STROKE MODELS

A. Expression of representative engineering models

Fundamental engineering models of lightning return stroke is expressed by the following equation:

$$I(z',t) = u(t - z'/v_f)\, P(z',t)\, I(0, t - z'/v) \cdots\cdots\cdots (27)$$

where $I(z',t)$ is the channel current at an arbitrart hight z' and arbitrary time t; $I(0,t)$ is the channel-base current; $u(t)$ is the Heaviside function; $P(z',t)$ is the heigh- and time-dependent coefficient; v_f is the return-stroke speed; v is the current-wave propagation speed.

Table II summarizes $P(z',t)$ and v for representative engineering models: the TL model [7], the modified TL model with exponential current decay (MTLE) [8], and the TCS [9] models. Fig. 3 shows conceptual pictures of TL and TCS models.

B. Proposed engineering model

A new engineering model of the lightning return stroke is given as follows:

$$I(z',t) = u(t - z'/v_f) I(0, t + z/c) \left[1 - \exp\left(\frac{1 - z/v_f}{\tau} \frac{\lambda_p}{z}\right)\right] \exp(-z/\lambda) \cdots\cdots\cdots (28)$$

This model considers both attenuation and dispersion of a lightning return-stroke current wave with its upward propagation along the channel. Fig. 4 shows waveforms of the channel current at different heights calculated using the proposed model for $\tau = 3$ μs, $\lambda_p = 1000$ m, $z = 1000$ m and $\lambda_p = 1000$ m. Fig. 4 also shows current waveforms calculated using the TL model for reference.

TABLE II
$P(z', t)$ AND FOR ENGINEERING MODELS

Model	$P(z', t)$	v
TL [8]	1	v_f
TCS [10]	1	$-c$
MTLE [9]	$\exp(-z'/\lambda)$	v_f

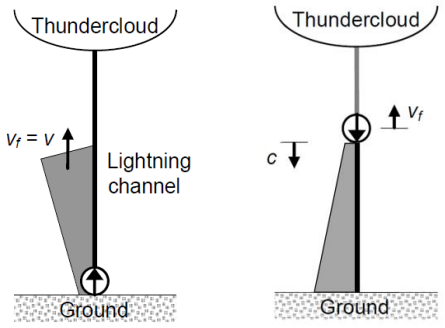

(a)TL model (b)TCS model

Fig. 3. Conceptual pictures for (a) the TL model, and (b) the TCS model.

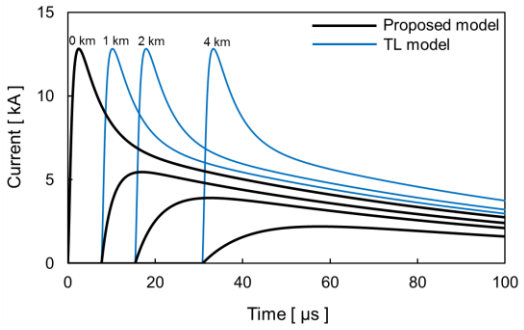

Fig. 4. Waveforms of current at different heights along a lightning return-stroke channel specified by TL and proposed models.

C. Typical features of LEMP waveforms

The following five features have been identified from lightning electromagnetic field waveforms observed at various distances from lightning return strokes [10][11]:

(a) characteristic flattening in about 15 μs of vertical electric fields at tens to hundreds of meters [11];
(b) sharp initial peak in both electric and magnetic fields;
(c) slow ramp following the initial peak for electric fields measured within few tens of kilometers;
(d) hump following the initial peak in magnetic fields within several tens of kilometers;
(e) zero crossing within tens of microseconds of the initial peak in both electric and magnetic fields at 50 to 200 km.

These features are illustrated in Fig. 5. They have been used as a benchmark for the validation of return stroke models [12][13].

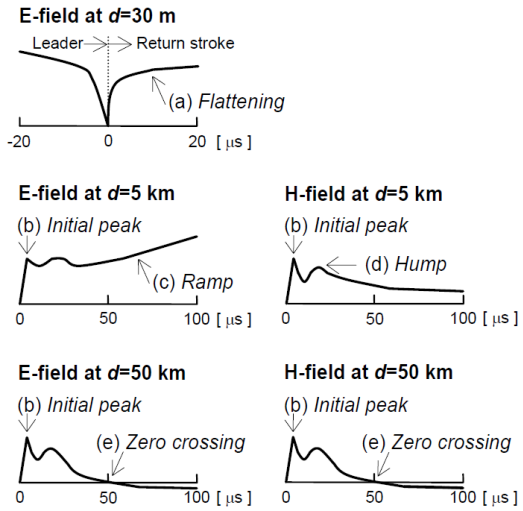

Fig. 5. Features found in typical measured vertical electric and azimuthal magnetic field waveforms associated with first and subsequent return strokes [11][12].

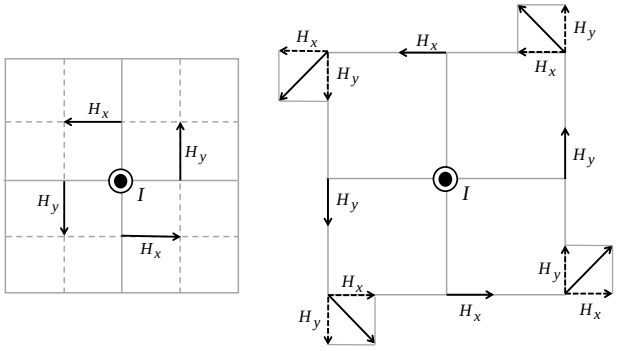

(a)FDTD method (b)CIP model

Fig. 6. Magnetic-field excitation locations for representing a current source in FDTD and CIP simulations.

TABLE III
CONDITIONS EMPLOYED IN CIP AND FDTD COMPUTATIONS

	(i) 100 m	(ii), (iv) 3 km	(iii) 100 km
Working space	1.2 x1.2 x2.0 km^3	13 x13 x15 km^3	400x400x100 km^3
Cell size	5 x5 x5 m^3	50 x50 x50 m^3	1 x1 x1 km^3
Time increments	9.53 ns	95.3 ns	1.91 μs
Time-max	15 μs	80 μs	600 μs

D. *Computed LEMP waveforms*

In this section, vertical electric field E_z and azimuthal magnetic field H_φ, generated by a current wave propagating along a vertical channel located on flat perfectly conducting ground, are computed using the CIP and FDTD method for TL, TCS, MTLE and proposed models.

In the FDTD simulation, a current source is represented by specifying its nearest circulating four magnetic fields as shown in Fig. 6 (a). In the CIP simulation, a current source is represented by specifying its first and second nearest twelve magnetic fields as shown in Fig. 6 (b).

The peak of the channel-base current is set to 13 kA, and its risetime is set to 1 μs. The return-stroke wavefront speed is set to 130 m/μs. Fig. 4 shows waveforms of current at heights 0 m, 1 km, 2 km and 4 km along the simulated lightning channel specified by TL and the proposed models. Table III shows conditions for computing (i) E_z at distance 100 m from the lightning channel, (ii) E_z at 3 km, (iii) E_z at 100 km, and (iv) H_φ at 3 km.

Fig. 7 shows CIP- and FDTD-computed waveforms of E_z at horizontal distance 100 m, 3 km and 100 km and H_φ at horizontal distance 3 km for the TL model. Figs. 8, 9 and 10 show those computed for TCS, MTLE and proposed models, respectively.

CIP-computed electromagnetic-field waveforms do not include non-physical-based oscillations, while FDTD-computed waveforms do. Particularly FDTD-computed waveforms for the TCS model include oscillations since the model involves a step-like rise at the wavefront. Even in the case like this, the CIP computation is stable.

Further, CIP-computed electromagnetic-field waveforms reproduce all the features of measured typical lightning electromagnetic-field waveforms, while the TL model cannot reproduce features (a), (c) and (e), the MTLE model cannot reproduce features (a) and (d), and the TCS model cannot reproduce feature (a). The latter conclusion agrees with that found in [12][13].

IV. CONCLUSIONS

The CIP method has been applied to computing LEMPs with representative engineering models of the lightning return stroke and a new model, and the CIP-computed LEMP waveforms have been compared with the corresponding FDTD-computed waveforms. It turns out that the CIP method is more stable than the FDTD method, and it yields more accurate results. Further, it is shown that LEMP waveforms at different distances from a lightning return-stroke channel, computed using the CIP method for the proposed lightning return-stroke model, agree reasonably well with the corresponding measured LEMP waveforms.

V. REFERENCES

[1] IEEJ Investigation Committee on Numerical Electromagnetic Field Analysis Methods for Surge Phenomena: Numerical Methods for Analyzing Transient Electromagnetic Fields, IEEJ (2008) (in Japanese)

[2] K. S. Yee: "Numerical solution of initial boundary value problems involving Maxwell's equations in isotropic media," IEEE Trans. AP, vol. 14, no. 8, pp. 320-307 (1966)

[3] R. F. Harrington: Field Computation by Moment Methods, Macmillan Co., New York (1968)

[4] T. Yabe, X. Feng, and T. Utsumi: "The constrained interpolation method for multiphase analysis," J. Computat. Phys., vol. 169, pp. 556-593 (2001)

[5] K. Okubo, and N. Takeuchi: "Analysis of an electromagnetic field created by line current using constrained interpolation profile method," IEEE Trans. AP, vol. 55, no. 1, pp. 111-119 (2007)

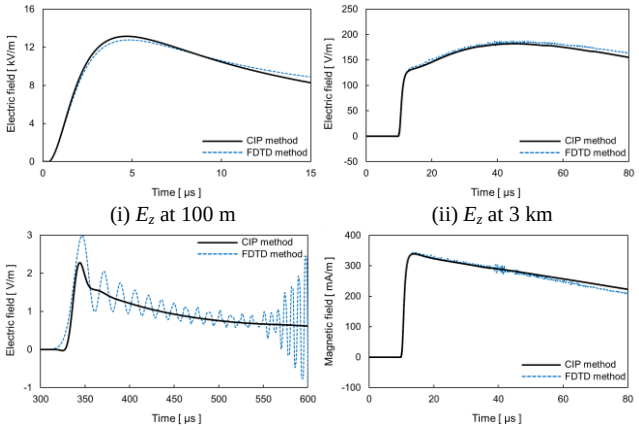

(i) E_z at 100 m (ii) E_z at 3 km

(iii) E_z at 100 km (iv) H_φ at 3 km

Fig. 7. E_z and H_φ at various distances computed for the TL model.

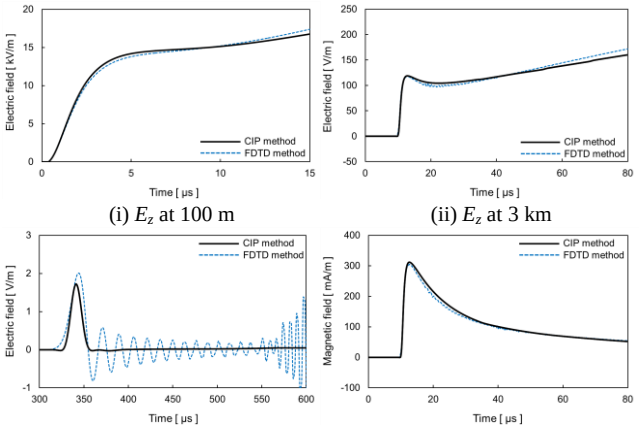

(i) E_z at 100 m (ii) E_z at 3 km

(iii) E_z at 100 km (iv) H_φ at 3 km

Fig. 9. E_z and H_φ at various distances computed for the MTLE model.

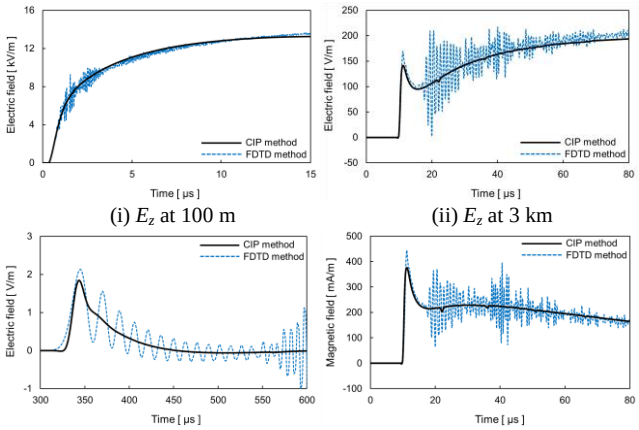

(i) E_z at 100 m (ii) E_z at 3 km

(iii) E_z at 100 km (iv) H_φ at 3 km

Fig. 8. E_z and H_φ at various distances computed for the TCS model.

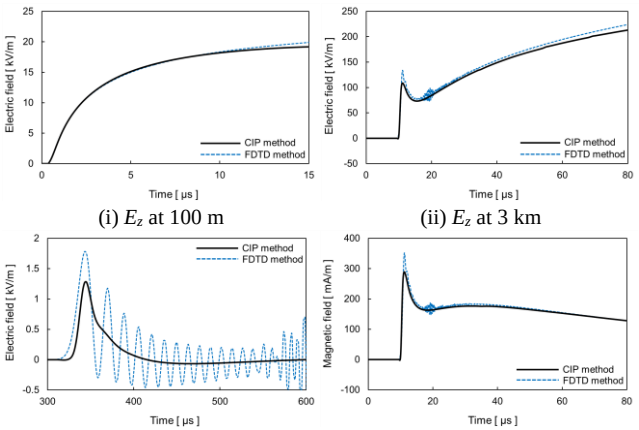

(i) E_z at 100 m (ii) E_z at 3 km

(iii) E_z at 100 km (iv) H_φ at 3 km

Fig. 10. E_z and H_φ at various distances computed for the proposed model.

[6] K. Kajita, K. Miyagawa, Y. Baba, N. Nagaoka, A. Ametani, J. Takami, and S. Okabe: "Application of the type-C constrained interpolation profile method to lightning electromagnetic field analyses," IEEJ Trans. PE, vol. 133, no.1, pp.106-113 (2013)

[7] M. A. Uman, D. K. McLain, and E. P. Krider: "The electromagnetic radiation from a finite antenna, " Amer. J. Phys., vol. 43, pp. 33-38 (1975)

[8] C. A. Nucci, C. Mazzetti, F. Rachidi, and M. Ianoz: "On lightning return stroke models for LEMP calculations, " in Proc. 19th Int. Conf. Lightning

[9] F. Heidler: "Traveling current source model for LEMP calculation," in Proc. 6th Int. Symp. EMC, Zurich, Switzerland, pp. 157-162 (1985)

[10] Y. T. Lin, M. A. Uman, J. A. Tiller, R. D. Brantley, W. H. Beasley, E. P. Krider, and C. D. Weidam: "Characterization of lightning return stroke electric and magnetic fields from simultaneous two-station measurements, " J. Geophys. Res., vol. 84, no. C10, pp. 6307-6314 (1979)

[11] M. A. Uman, V. A. Rakov, J. A. Veraggi, R. Thottappillil, A. EybertBerard, L. Barret, J.-P. Berlandis, B. Bador, P. P. Barker, S. P. Hant, J. P. Oravsky, T. A. Short, C. A. Warren, and R. Bernstein: "Electric fields close to triggered lightning," in Proc. EMC ROMA Symp., pp. 33-37, Rome, Italy (1994)

[12] V. A. Rakov and M. A. Uman, "Review and evaluation of lightning return stroke models including some aspects of their application, " IEEE Trans. EMC, vol. 40, pp. 403-426 (1998)

[13] Y. Baba, S. Miyazaki and M. Ishii, "Reproduction of lightning electromagnetic field waveforms by engineering model of return stroke," IEEE Trans. EMC, vol. 46, no.1 (2004)